Inhibitory selectivity among class I HDACs has a major impact on inflammatory gene expression in macrophages

Cao, Fangyuan; Zwinderman, Martijn; van Merkerk, Ronald; Ettema, Petra; Quax, Wim; Dekker, Frank J.

Published in:
European Journal of Medicinal Chemistry

DOI:
10.1016/j.ejmech.2019.05.038

Publication date:
2019

European Journal of Medicinal Chemistry 177 (2019) 457–466

Contents lists available at ScienceDirect

European Journal of Medicinal Chemistry

journal homepage: http://www.elsevier.com/locate/ejmech

Research paper

Inhibitory selectivity among class I HDACs has a major impact on inflammatory gene expression in macrophages

Fangyuan Cao, Martijn R.H. Zwinderman, Ronald van Merkerk, Petra E. Ettema, Wim J. Quax, Frank J. Dekker*

Chemical and Pharmaceutical Biology, Groningen Research Institute of Pharmacy (GRIP), University of Groningen, Groningen, 9713 AV, the Netherlands

ARTICLE INFO

Article history:
Received 10 April 2019
Received in revised form
10 May 2019
Accepted 13 May 2019
Available online 18 May 2019

Keywords:
Histone deacetylases inhibitors (HDACi)
Entinostat
NF-κB activity
Inflammation

ABSTRACT

Histone deacetylases (HDACs) play an important role in cancer, degenerative diseases and inflammation. The currently applied HDAC inhibitors in the clinic lack selectivity among HDAC isoforms, which limits their application for novel indications such as inflammatory diseases. Recent, literature indicates that HDAC 3 plays an important role among class I HDACs in gene expression in inflammation. In this perspective, the development and understanding of inhibitory selectivity among HDACs 1, 2 and 3 and their respective influence on gene expression need to be characterized to facilitate drug discovery. Towards this aim, we synthesized nine structural analogues of the class I HDAC inhibitor Entinostat and investigated their selectivity profile among HDACs 1, 2 and 3. We found that we can explain the observed structure activity relationships by small structural and conformational differences between HDAC 1 and HDAC 3 in the 'lid' interacting region. Cell-based studies indicated, however, that application of inhibitors with improved HDAC 3 selectivity did not provide an anti-inflammatory response in contrast to expectations from biochemical evidence in literature. Altogether, in this study, we identified structure activity relationships among class I HDACs and we connected isoform selectivity among class I HDACs with pro- and anti-inflammatory gene transcription in macrophages.

1. Introduction

Histone deacetylases (HDACs) play an important role in cancer, degenerative diseases and inflammation. Currently, HDAC inhibitors are in clinical use for the treatment of cancer. However, they often lack selectivity among HDAC isoforms, which limits their application for novel indications such as inflammatory diseases. Recent literature indicates that HDAC 3 plays an important role among class I HDACs in gene expression in inflammation (as reviewed [1]). In this perspective, the development and understanding of inhibitory selectivity among HDACs 1, 2 and 3 and their respective influence on gene expression need to be characterized to facilitate drug discovery.

HDACs are a family of enzymes that deacetylate lysine residues of histones and non-histone proteins. Deacetylation of lysine residues in histones leads to a more condensed chromatin structure and makes DNA less accessible for gene transcription [2]. To date, eighteen HDAC isoenzymes have been identified, and they are divided into four classes based on their structural similarity [3,4]. Class I HDACs, which include zinc-dependent HDAC 1, 2, 3 and 8, are well-known for their importance in gene expression, survival, and proliferation in cells [5]. Therefore, small molecule inhibitors of class I HDACs have been considered as potential therapeutics in cancer [6], neurological disorders [7], inflammatory diseases [8] and also cardiac and pulmonary diseases [4]. Most of the currently available HDAC inhibitors share the same structural characteristics i.e. they contain: 1) a zinc-binding group (ZBG) to bind the zinc ion of the active site of class I HDACs, 2) a linker part that mimics the lysine side chain and 3) a cap group that binds to the edge of active site (see Fig. 1). In our study, we selected Entinostat as a class I selective HDAC inhibitor to explore structure activity relationships for selectivity among class I HDAC isoforms and its respective influence on pro- and anti-inflammatory gene expression in macrophages.

It has been shown that HDACs are important regulators in immune responses [9,10]. Therefore, development of HDAC inhibitors as new immunomodulatory therapeutics holds promise for development of therapeutics in inflammation [11] and cancer [12,13].

* Corresponding author.
E-mail address: f.j.dekker@rug.nl (F.J. Dekker).

https://doi.org/10.1016/j.ejmech.2019.05.038
0223-5234/

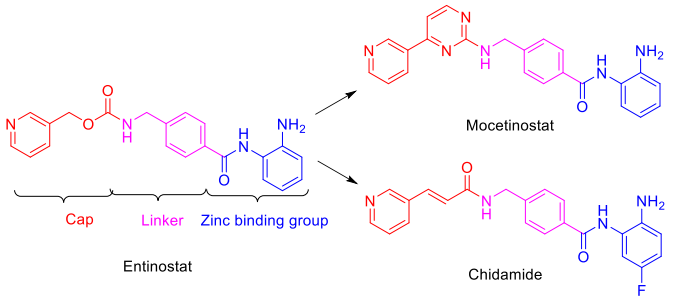

Fig. 1. Chemical structures of HDAC inhibitors with an *o*-aminoanilide core structure Entinostat, Mocetinostat and Chidamide. The general design of HDAC inhibitors with a zinc binding group (blue), a linker (pink) and a cap (red) is shown. (For interpretation of the references to color in this figure legend, the reader is referred to the Web version of this article.)

Interestingly, there are currently several clinical trials ongoing that aim to evaluate the synergy for combination of HDAC inhibitors and immune therapies in cancer [12,13]. Increasing evidence indicates that HDAC inhibitors play key roles in regulation of immune cells in their respective microenvironment in immune reactions [13,14]. Key players in the immune microenvironment are macrophages, which can secrete both pro-inflammatory cytokines such as Tumor Necrosis Factor-α (TNF-α) and anti-inflammatory cytokines such as Interleukin-10 (IL-10) [15,16].

In the context of airway inflammation, our previous works demonstrates that the class I HDAC inhibitor Entinostat has anti-inflammatory effects upon cigarette smoke exposure *in vivo* in a mouse model. The anti-inflammatory effect observed in mice could mechanistically be explained by *in vitro* studies in Lipopolysaccharides (LPS)/Interferon γ (INFγ) - stimulated murine RAW 264.7 macrophages. Upon Entinostat treatment increased acetylation of the nuclear factor-κB (NF-κB) transcription factor, increased nuclear localization and increased binding to the IL-10 promotor region was observed. This provides a mechanistic explanation of the observed upregulation of IL-10 expression, which is an anti-inflammatory cytokine [8]. Nevertheless, in the murine macrophage model we found upregulation of the expression of both pro- and anti-inflammatory genes [8], which indicates a mixed effect *in vitro*. The observed effects on the expression of both pro- and anti-inflammatory genes by the class I HDAC inhibitor Entinostat call for further investigation of the role of HDAC inhibitor selectivity in the regulation of pro- and anti-inflammatory gene expression.

Here, we synthesized several analogues of Entinostat and investigated the selectivity profile of these analogues among class I HDACs 1, 2 and 3 and their effects on pro- and anti-inflammatory gene expression. Structure activity relationship (SAR) for small structural variations in the area between the linker and the lid region of the inhibitor were investigated. Subsequently, the influence of HDAC inhibitor selectivity on inflammatory gene expression was assessed using LPS/INFγ-stimulated murine macrophages.

2. Results and discussion

2.1. Synthesis

The synthetic routes to obtain the desired compounds are outlined in Schemes 1–3. The *o*-aminoanilide derivatives **4a**, **4b** and **4d** were prepared in two steps (Scheme 1). A reductive amination reaction was used to obtain **3a**, **3b** and **3d** with yields between 45% and 75%. Amide **3c** was prepared from 4-(methoxycarbonyl)benzoic acid and aniline by a condensation reaction using EDCI and HOBt as reagents in a yield of 81%, followed by hydrolysis of the

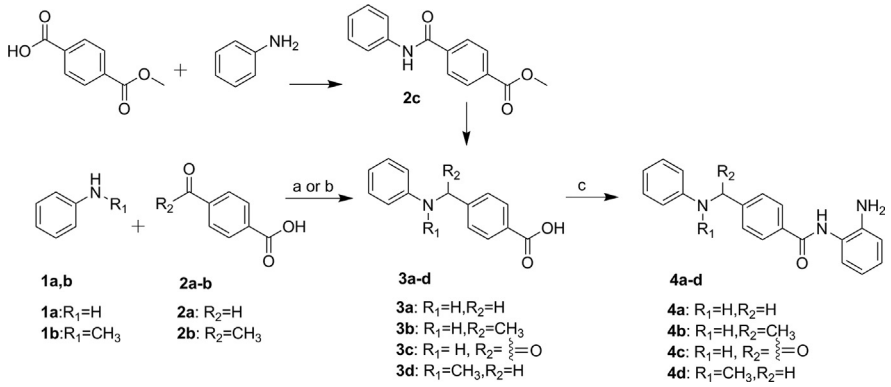

Scheme 1. Reagents and conditions: a) EDCI, HOBt, CH_2Cl_2, Et_3N,r.t. overnight; b) LiOH, CH_2Cl_2, r.t., 3 h; c) 50 °C, 6 h; $NaBH_3CN$, methanol, r.t., overnight; d) *o*-phenylenediamine, EDCI, HOBt, DCM, Et_3N, r.t. overnight.

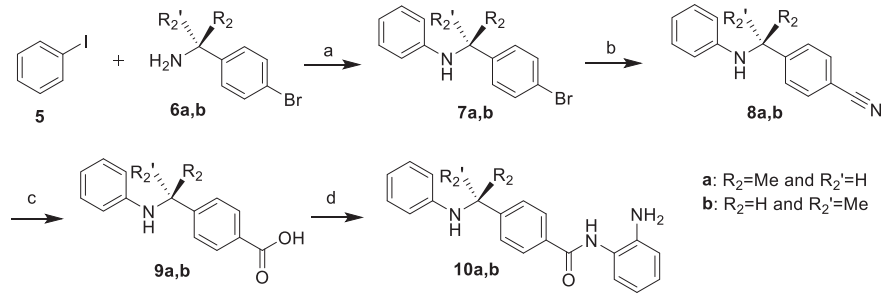

Scheme 2. Reagent and conditions: a) K_2CO_3, L-Proline, CuI, DMSO, 80 °C, overnight; b) $Zn(CN)_2$, $Pd(PPh_3)_4$, DMF, 105 °C, overnight; c) 12 N HCL, 100 °C, overnight; d) EDCI, HOBt, CH_2Cl_2, r.t., overnight.

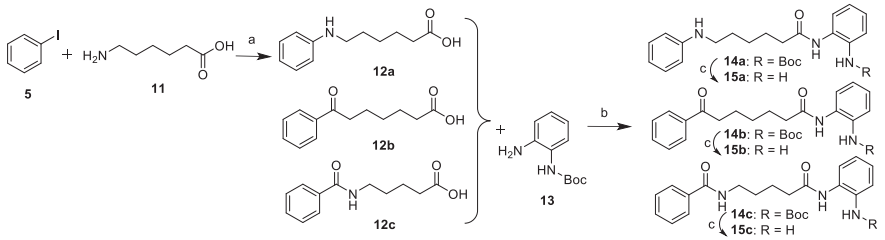

Scheme 3. Reagents and conditions:a) CuI, K_2CO_3, deanol, H_2O, 85 °C, overnight; b) EDCI, HOBt, CH_2Cl_2, r.t. overnight; c) TFA, CH_2Cl_2, r.t. 2 h.

ester using lithium hydroxide to obtain compound **4c** in a yield of 54%. Compounds **4a-d** were obtained by a condensation reaction from **3a-d** with *o*-phenylenediamine using EDCI and HOBt as reagents in a yield of 30%–61%.

The pure enantiomers of **4b** were prepared in four steps starting from commercially available (R)-(+)- or (S)-(−)-1-(4-bromophenyl)ethylamine and iodobenzene (Scheme 2). The first step was done by an Ullmann reaction to couple 1-(4-bromophenyl)ethylamine and iodobenzene using L-proline and CuI to give **7a** and **7b** with yields around 33%. Compounds **7a** and **7b** were subjected to cyanation using zinc cyanide with tetrakis(-triphenylphosphine)palladium(0) as catalyst to obtain **8a** and **8b** with a yield of about 57%. The cyanides **8a** and **8b** were hydrolyzed and coupled with *o*-phenylenediamine to obtain desired compounds **10a** and **10b** in a yield of around 30%.

Compounds **15a-c** were obtained in two or three steps (Scheme 3). Compound **12a** was produced by using an Ullmann reaction in which 6-aminohexanoic acid and phenyliodide were coupled using deanol and CuI in alkaline conditions [17]. Carboxylates **12a-c** were coupled with *N*-Boc-1,2-phenylenediamnie to give the Boc protected **14a-c** with low to moderate yields (6–66%). Boc deprotection was achieved by trifluoroacetic acid treatment to obtain the final product **15a-c**.

2.2. HDAC inhibition

The resulting collection of HDAC inhibitors was tested for HDAC inhibition using procedures to assay HDAC activity as described previously by us [18] and others. The IC_{50} values of HDAC inhibitors for HDAC 1, 2 and 3 are listed in Table 1 and 2. In line with prior reports, Entinostat provided IC_{50}'s in the nM range [8,19]. The structure activity relationships show that replacement of the 'lid' region of Entinostat by a phenyl, as present in **4a**, results in a loss of potency for HDAC 1 and 2, whereas the HDAC 3 inhibition remains similar. Using the compound collection **4a**, **4b**, **4c** and **4d**, we probed the selectivity profile among HDACs 1, 2 and 3 (Table 1) by variation of the benzylic position between the 'linker' and the 'lid' region. We observed that introduction of a methyl or a carbonyl in the benzylic position provides inhibitors **4b** and **4c** with respectively 10- or 20-fold reduced inhibitory potency for HDAC 3 compared to much smaller changes for HDAC 1 and 2. Introduction of a methyl on the benzylamine nitrogen in **4d** provides much smaller changes in affinity. The two enantiomers of **4b** are also tested for HDAC 1, 2 and 3 inhibition. The IC_{50} values show that S-(−)enantiomer **10a** and R-(+)-enantiomer **10b** are displaying the same selective profile among HDACs 1, 2 and 3, but R-(+)-enantiomer **10b** shows 2 times better inhibitory potency.

Based on prior literature [20], we set out to explore a series of compounds **15a-c** with HDAC 3 inhibitory selectivity (Table 2). Compound **15a** shows the highest potency for HDAC 3, whereas **15b** has equal IC_{50}'s for HDAC 1 and 3. Compound **15c** has the clearest selectivity profile with the highest potency for HDAC 3 in the same range as RGFP966.

Table 1
IC_{50} values of Entinostat and **4a-d** for HDAC 1, HDAC 2 and HDAC 3. Data are presented as mean values (in μM) ± SD.

Name	Structure	HDAC 1	HDAC 2	HDAC 3
Entinostat[a]	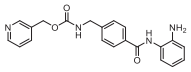	0.19 ± 0.04	0.41 ± 0.09	0.95 ± 0.19
4a	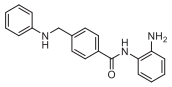	1.0 ± 0.1	1.4 ± 0.05	0.6 ± 0.05
4b	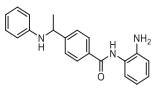	2,3 ± 0.2	7.0 ± 0.5	8,5 ± 0.5
10a	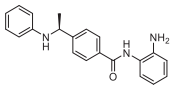	2.4 ± 0.6	8.3 ± 0.8	11 ± 0.7
10b	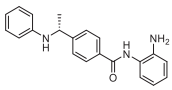	1.3 ± 0.1	4,2 ± 0.6	5.0 ± 0.1
4c	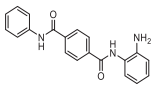	3.0 ± 0.4	5.4 ± 0.3	16 ± 2.2
4d	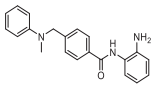	1.0 ± 0.03	0.5 ± 0.01	2.8 ± 0.06

[a] IC_{50} values for Entinostat are taken from Leus et al., 2017.

Table 2
IC_{50} values of RGFP966 and compound 15a-c for HDAC 1, 2 and 3. Data are presented as mean values. (in μM) ± SD.

Name	Structure	HDAC 1	HDAC 2	HDAC 3
RGFP966[a]	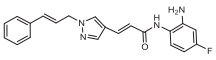	5.6 ± 1.3	9.7 ± 1.8	0.21 ± 0.06
15a	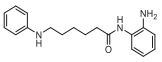	1.2 ± 0.2	1.3 ± 0.3	0.4 ± 0.05
15b	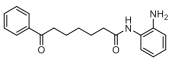	1.9 ± 0.1	3.7 ± 0.7	1.2 ± 0.1
15c	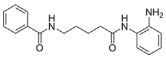	4.2 ± 0.8	8.1 ± 1.5	0.6 ± 0.07

[a] IC_{50} values for RGFP966 are taken from Leus et al., 2016.

2.3. Docking studies

A molecular modelling study was performed to connect the observed SAR among class I HDACs 1, 2 and 3 to structural

information. Towards this aim a selection of the inhibitors was docked into the active sites of HDACs by the program Discovery studio (Dassault systèmes) version 2018, using the crystal structures of human HDAC 1 (PDB-code: 5ICN), human HDAC 2 (PDB-code: 4LY1) and human HDAC 3 (PDB-code: 4A69). The CDOCKER protocol was employed for docking by a CHARMm based algorithm. This docking protocol was verified by redocking of the ligand (4-(acetylamino)-*N*-[2-amino-5-(thiophen-2-yl)phenyl]benzamide) from the HDAC 2 crystal structure [21]. The ligand was removed from the HDAC 2 crystal structure, and then, was docked back using the CDOCKER protocol. This provides positions comparable to the original binding pose in all top 10 lowest CDOCKER energy poses [21], thus confirming that the docking protocol can recapitulate the binding pose in the crystal structure of HDAC 2. Next, we verified the docking protocol for HDAC 1 and 3. We made an overlay of HDAC 1, 2 and 3 on the α-carbon atoms of the protein backbone and copied the ligand (4-(acetylamino)-*N*-[2-amino-5-(thiophen-2-yl)phenyl] benzamide) from the HDAC 2 crystal structure 4YL1 into the active sites of HDAC 1 and 3. Subsequently, the *o*-aminoanilide core was used as a reference to evaluate the docking of the inhibitors into the HDAC 1 and 3 active sites. We found that the docking protocol enables positioning of *o*-aminoanilide core of the novel inhibitors in HDAC 1 and 3 active site with poses that are very similar to the pose of *o*-aminoanilide core of the reference inhibitor in HDAC 2. The top 10 CDOCKER energies poses were visually inspected and poses in which the *o*-aminoanilide core docked outside the active site were discarded. For all the ligands a high convergence in the position of *o*-aminoanilide core was observed in the 10 highest ranked poses (examples are shown in Figs. S1 and S2). Poses with the lowest CDOCKER energies are shown as representative poses in all figures (see Fig. 2).

Firstly, we performed a docking analysis to find an explanation for the 20-fold difference in HDAC 3 inhibitory potency between **4a** and **4c** (Fig. 2A). The amine and carbonyl of *o*-aminoanilide group in both the reference ligand and tested compounds are embedded in the active site to chelate the zinc ion in the catalytic center. The phenyl linker moiety of both compounds forms π-π stacking with Phe144 and Phe 200 in HDAC 3 to fit the hydrophobic tunnel of the active site. Interestingly, the docking indicates that compound **4c** with the amide group instead of a benzylic nitrogen between the 'linker' and the 'lid' does not interact in the 'lid' region with the protein surface in contrast to **4a**. The amide linkage is connected to a 10-fold loss in potency for HDAC 3 and not for HDAC 1 and 2, thereby indicating that binding of the phenyl to the lid region is key for HDAC 3 binding in contrast to HDAC 1 and 2.

Based on the idea that flexibility is key for HDAC 3 binding we explored a set of compounds with a flexible linker (Table 2). Because of its clearest preference for binding to HDAC 3, we focused on compound **15c**. This molecule was docked in the active site of HDAC 1 and 3 and superimposed (Fig. 2B). Using this docking we compared the position of the amino acids in the respective HDAC active sites. A high degree of overlap in the amino acids of the HDAC 1 and HDAC 3 active sites was observed as well as in the docked conformation of **15c**. The only exception is amino acid Asp93 in HDAC 3 compared with Asp99 in HDAC 1 for which the α-carbon atom as well as the amino acid side chain occupy alternative positions. The carboxylic acid of Asp99 in HDAC 1 is located more towards the outside of active site than Asp93 in HDAC 3. This positional and conformational difference can be attributed to the difference between Glu98 in HDAC 1 and Asp92 in HDAC 3. In the crystal structure, Asp99 in HDAC 1 is hydrogen bonded with three water molecules (Fig. 2C), whereas Asp93 in HDAC 3 is only hydrogen bonded to one water molecule (Fig. 2D). This could contribute to a higher propensity for hydrogen bonding to Asp92 in HDAC 3 compared to Asp99 in HDAC 1 thus resulting in a high affinity of compound **15c** for HDAC 3 compared to HDAC 1. Thus, the positional difference between Asp99 in HDAC 1 and Asp92 in HDAC 3 provides a structural basis to design inhibitors with selectivity among these HDAC isoenzymes by targeting the region between the 'linker' and the 'lid' region of the inhibitors. This adds to the structural understanding of inhibitor selectivity among HDAC 1, 2 and 3, which is, currently, largely focused on the 'zinc binding group' region [22–25].

2.4. NF-κB activation

It is known that NF-κB is an important regulator in cytokine secretion of macrophages [18,26]. Our previous study has shown that Entinostat restored anti-inflammatory IL-10 expression in LPS/INFγ-treated macrophages, which is connected to increased NF-κB p65 transcriptional activity, acetylation, nuclear localization, and binding to the IL-10 promoter [8]. Therefore, we aimed to connect HDAC isoenzyme selectivity to effects on NF-κB transcriptional activity. Inhibitors with different HDAC selectivity profiles were tested for their effect on NF-κB transcriptional activity using a reporter gene assay with RAW-Blue cells. LPS/IFNγ-stimulated RAW-Blue cells were treated with compounds at non-toxic concentrations ranging between 1 and 5 μM (data on cell viability are shown in the supporting information). The pan-HDAC inhibitor SAHA was used as a reference. As shown in Fig. 3, both Entinostat and **10b** upregulated the NF-κB transcriptional activity, whereas RGFP966 and **15c** did not show obvious effects on reporter gene expression at the concentrations applied. Both Entinostat and compound **10b** have a preference for HDAC 1 inhibition compared to a preference for HDAC 3 for RGFP966 and **15c**. These results indicate that HDAC 1 inhibition, rather than HDAC 3 inhibition, plays an essential role in the NF-κB transcriptional activation in this model.

2.5. Gene expression

Subsequently, we investigated the effect of HDAC inhibitors with different selectivity's among HDAC 1, 2 and 3 isoenzymes on pro- and anti-inflammatory gene expression. We employed LPS/IFNγ-stimulated RAW264.7 cells to monitor expression of tumor necrosis factor α (TNFα), interleukin-6 (IL-6) and inducible nitric oxide synthase (iNOS) as pro-inflammatory genes and expression of IL-10 as anti-inflammatory gene (see Fig. 4) [8]. As observed previously, Entinostat increased the expression of both pro- and anti-inflammatory genes. This effect was also observed using the inhibitor **4b**, which also preferably inhibits HDAC 1 (despite at higher concentrations compared to Entinostat due to a lower inhibitory potency). On the contrary, inhibitors with a preference for HDAC 3 inhibition did not show significant effects on gene expression. These results indicate that small molecule inhibition of HDAC 3 may not be strongly connected with regulation of pro- and anti-inflammatory gene expression in this model. This in contrast to previous findings with siRNA mediated downregulation of HDAC 3 downregulated pro-inflammatory gene expression and upregulated expression of IL-10 [27]. Possibly, the structural role of HDAC 3 is more important than its catalytic activity in regulation of pro- and anti-inflammatory gene expression. On the contrary, this study shows that inhibition of the catalytic activity of HDAC 1 -and/or HDAC 2 is associated with expression of both pro-inflammatory and anti-inflammatory genes. This indicates a crucial role for the HDAC 1 and HDAC 2 isoforms in the function of macrophages. The stimulation of pro-inflammatory gene expression by HDAC 1 and/or 2 directed inhibitors indicates a role in activation of the immune system that could be beneficial in immunotherapy.

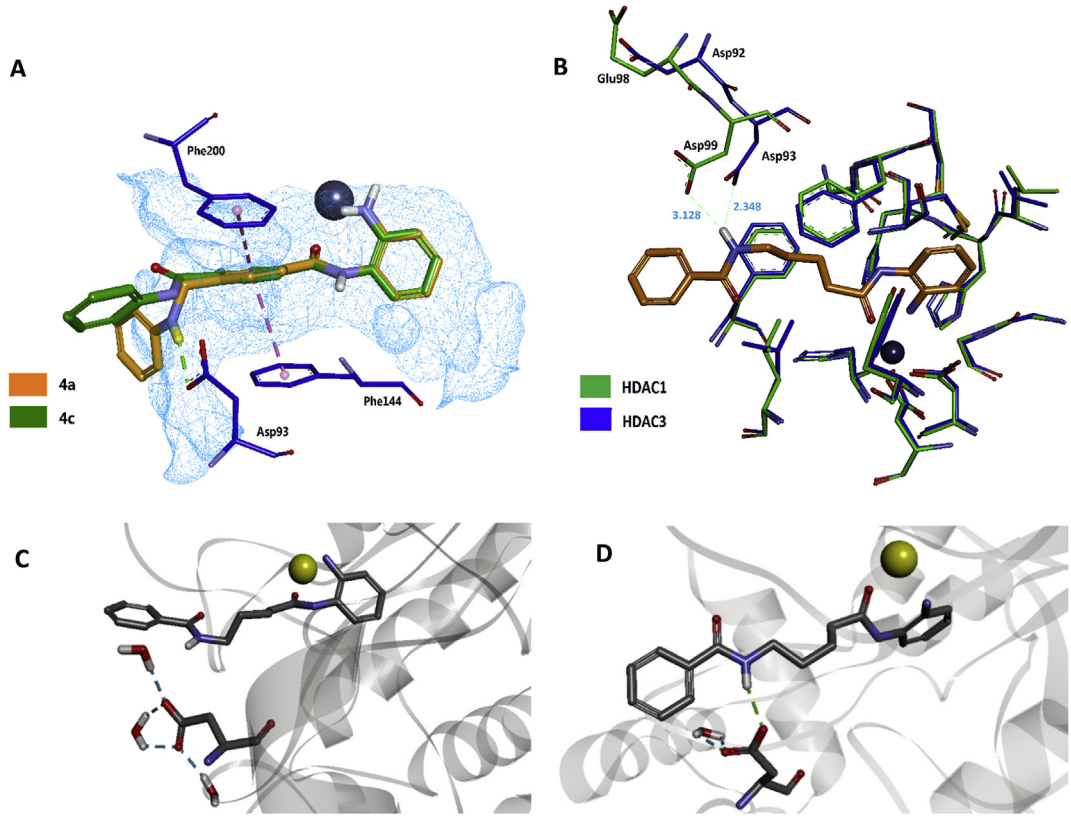

Fig. 2. Docking HDAC inhibitors in the active sites of HDAC 1 and 3. A) Modelling of **4a** and **4c** in the active site of HDAC 3. **4a** is colored in orange, and **4c** is colored in green. The blue mesh indicates the active site surface of HDAC 3, with a grey-colored zinc atom. B) Alignment of HDAC 1 and 3 structures docked with compound **15c**. HDAC 1 is labeled in green, and HDAC 3 is labeled in blue with a grey colored zinc atom. The distance between Asp99 in HDAC 1, while Asp93 in HDAC 3 and the compound is marked in light blue. C) Water coverage of Asp99 HDAC 1 in compound **15c** modelling. D) Water coverage of Asp93 HDAC 3 in compound **15c** modelling. (For interpretation of the references to color in this figure legend, the reader is referred to the Web version of this article.)

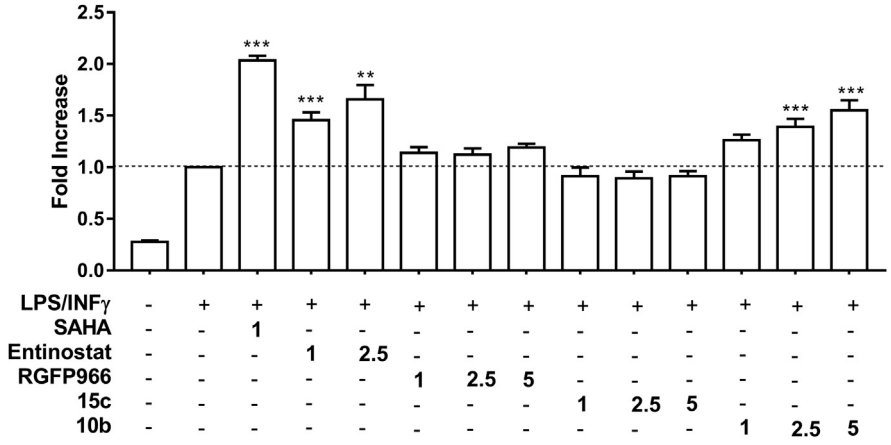

Fig. 3. Effect of SAHA, Entinostat, RGFP966, **10b** and **15c** on NF-κB transcriptional activity in LPS/IFNγ-stimulated RAW BLUE cells. Cells were treated with the respective HDAC inhibitors at the indicated concentrations for 20 h and stimulated with LPS/IFNγ for the last 4 h of the experiment. The data shown represent means ± SD of 3 independent experiments. ***$p < 0.001$ and **$p < 0.01$ compared to vehicle treated cells.

3. Conclusion

In this study, we set out to evaluate the structure activity relationships for selectivity among the HDACs 1, 2 and 3 by structural variation of the unit between the 'linker' and the 'lid' region of *o*-aminoanilide type HDAC inhibitors. We found that differences in HDAC 1 and HDAC 3 binding can be explained by a structural difference between HDAC 1 and HDAC 3. The Asp92 residue in HDAC 3 occupies a position that is different from the corresponding Asp99 residue in HDAC 1. The Asp92 in HDAC 3 is positioned closer to the tunnel towards the catalytic site, which could provide a higher propensity for hydrogen bonding, which would explain the 10-fold differences in potency for HDAC 3 inhibition as observed in this study. Subsequently, we set out to connect class I HDAC inhibitory selectivity to NF-κB transcriptional activity and pro- and anti-inflammatory gene expression. We found that HDAC 1 and/or

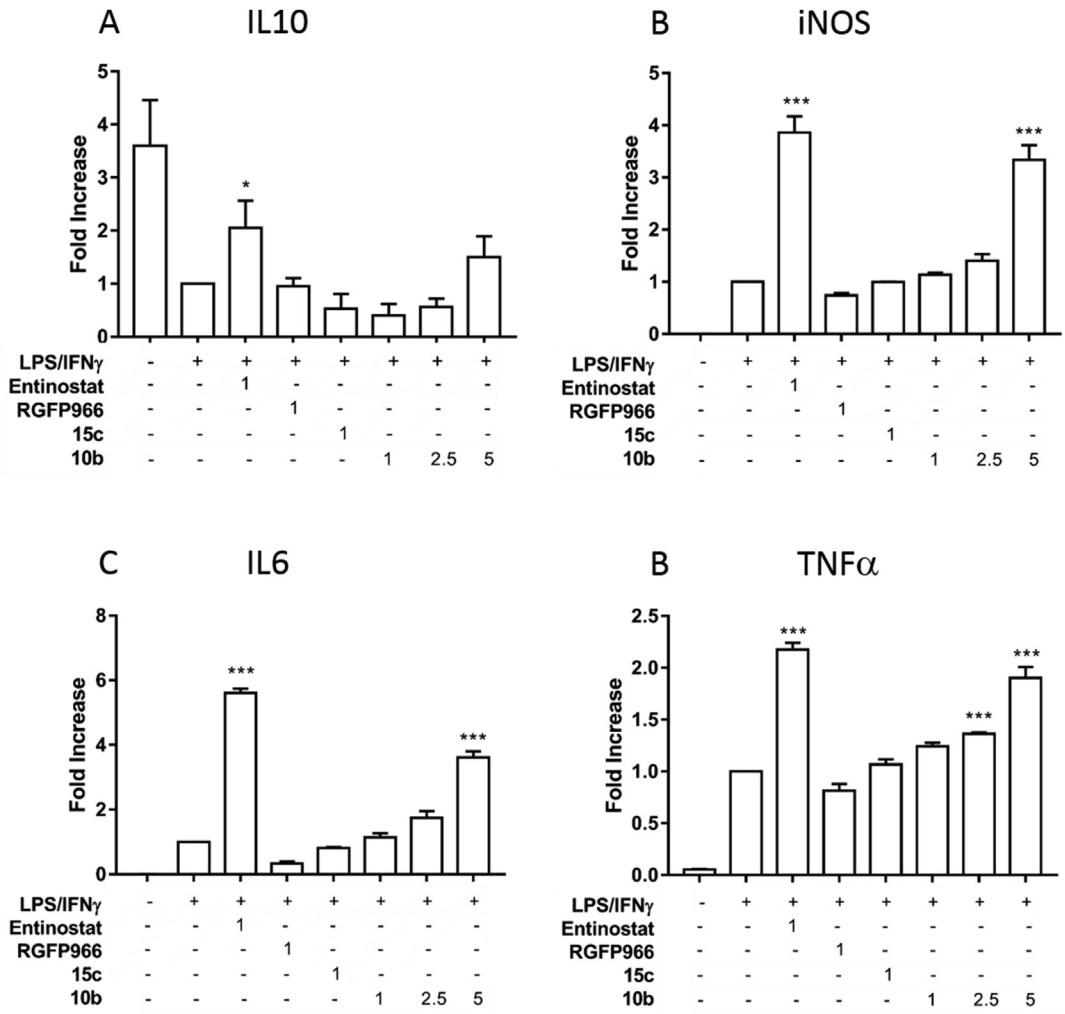

Fig. 4. Effects of Entinostat, RGFP966, **15c** and **10b** on pro- and anti-inflammatory gene expression of A) IL10, B) iNOS, C) IL6 and D) TNFα in RAW264.7 macrophages. Cells were treated with the respective HDAC inhibitors at the indicated concentrations for 20 h and stimulated with LPS/IFNγ for the last 4 h of the experiments. Gene expression was analyzed by RT-qPCR. For vehicle treatment, cells were pre-treated with a proportional dilution of the inhibitor solvent DMSO. Data are shown represent as mean values ± SD of 2–3 independent experiments. ***$p < 0.001$ compared to vehicle treated cells. *$p < 0.05$ compared to vehicle treated cells.

HDAC 2 selectivity increased the NF-κB transcriptional activity, whereas HDAC 3 selectivity provided no effect. The same was observed for both pro- and anti-inflammatory gene expression in which HDAC 1 and/or 2 selectivity upregulated gene expression, whereas HDAC 3 selectivity did not provide significant effects. The lack of effect observed with HDAC 3 selective inhibitors stand in contrast to previous studies employing siRNA downregulation, thus indicating a structural role for HDAC 3 in inflammatory signaling and not a catalytic role. Altogether, this study provides a basis to further explore isoenzyme selective class I HDAC inhibitors in applications involving immune regulation such as inflammatory disorders and oncology.

4. Experimental section

4.1. Chemistry

4.1.1. General

The solvents and reagents were purchased from Sigma-Aldrich, Acros chemicals or abcr GmbH without further purification. Reactions were monitored by thin layer chromatography (TLC). Merck silica gel 60 F254 plates were used and spots were detected under UV light or after staining with potassium permanganate for the non UV-active compounds. MP Ecochrom silica 32–63, 60 Å was used for flash column chromatography. ^{1}H NMR (500 MHz) and ^{13}C NMR (126 MHz) spectra were recorded with a Bruker Avance 4-channel NMR Spectrometer with TXI probe. Chemical shifts were referenced to the residual proton and carbon signal of the deuterated solvent $CDCl_3$: $\delta = 7.26$ ppm (^{1}H) and 77.05 ppm (^{13}C), $(CD_3)_2SO$: $\delta = 2.50$ ppm (^{1}H) and 39.52 ppm (^{13}C),CD_3OD: $\delta = 3.31$ ppm (^{1}H) and 49.00 ppm (^{13}C). The following abbreviations were used for spin multiplicity: s = singlet, br. s = broad singlet, d = doublet, t = triplet, q = quartet, p = quintet, dd = double of doublets, ddd = double of doublet of doublets, m = multiplet. Fourier Transform Mass Spectrometry (FTMS) was recorded on an Orbitrap XL Hybrid Ion Trap-Orbitrap Mass Spectrometer to give high-resolution mass spectra (HRMS).

4.1.2. Synthetic procedure 1: reductive amination

The respective substituted benzoic acid (4.0 mmol) was dissolved in MeOH (7.0 mL). The solution was heated to 50 °C and aniline (4.0 mmol) was added into the solution. Then a catalytic amount of acetic acid (10 drops) was added into the mixture. The reaction was stirred at 50 °C for 3 h. The mixture was then cooled to

room temperature. Molecular sieves and $NaBH_3CN$ (12 mmol) were added and stirring was continued for 16 h. The reaction was quenched with water (20 mL). The suspension was filtered, and the residue was washed with water (20 mL, 3 times) and dried to obtain the final product.

4.1.3. Synthetic procedure 2: amidation reaction

The respective carboxylic acid derivative (2 mmol) was added into a flask with dry CH_2Cl_2 (5 mL) and was put on ice. EDCI (2.4 mmol) and HOBt (0.8 mmol) were then added into the mixture and the reaction was stirred on ice for 15 min. Then Et_3N (2.0 mmol) was added into the mixture, followed the amine (2.0 mmol). Subsequently, the mixture was stirred at room temperature overnight. The reaction mixture was evaporated under reduced pressure. The residue was purified by flash chromatography using Petroleum ether: EtOAc 5:1 (v/v) as eluent, to obtain the final product.

4.1.4. Synthetic procedure 3: ester hydrolysis

Compound **3c** (3.8 mmol) was dissolved in THF:MeOH (8 mL: 4 mL) and a solution of LiOH (15 mmol) in water (8 mL) was added. The reaction was stirred at room temperature for 4 h until the solution became homogeneous. The reaction was acidified to pH 1.0 with an aqueous 1 N HCl solution. The solvents were evaporated under reduced pressure, and the residue was dissolved in the EtOAc:CH_2Cl_2 (15 mL:15 mL) and washed with water (20 mL, 3 times). The organic layers were combined, dried over $MgSO_4$ and evaporated to afford the final product.

4.1.5. Synthetic procedure 4: Ullmann reaction using L-proline

A mixture of iodobenzene (5.0 mmol), (S)- or (R)-4-bromophenylethylamine (5.0 mmol), K_2CO_3 (10 mmol), CuI (0.50 mmol) and L-proline (1.0 mmol) in DMSO (6 mL) was heated to 60 °C for 20 h. After cooling, the mixture was partitioned between water and EtOAc. The organic layer was separated, and the aqueous layer was extracted with EtOAc (10 mL). The combined organic layers were washed with brine (10 mL, 3 times), dried over $MgSO_4$, filtered, and concentrated under reduced pressure. The residual oil was purified by flash chromatography using Petroleum ether: EtOAc 15:1 (v/v) as eluent, to afford the product.

4.1.6. Synthetic procedure 5: cyanation reaction

The phenylbromide (1.5 mmol), $ZnCN_2$ (3.0 mmol), and Pd $[(C_6H_5)_3P]_4$ (0.15 mmol) were dissolved in anhydrous dimethylformamide (DMF) (4 mL) under a nitrogen atmosphere. The yellow mixture was heated to 105 °C for 28 h. Subsequently, the mixture was cooled to room temperature and an aqueous 1 N NaOH solution (10 mL) was added to quench the reaction. The mixture was extracted by CH_2Cl_2 (30 mL, 3 times). The organic layers were combined and washed with brine (30 mL, 3 times) and dried over $MgSO_4$. Subsequently, the solvent was removed under reduced pressure to afford the crude phenylcyanide product that was purified by flash chromatography (Petroleum ether: EtOAc 15:1(v/v)).

4.1.7. Synthetic procedure 6: acidic hydrolysis of nitriles

The phenylcyanide (0.40 mmol) was suspended in an aqueous 12 N HCl solution (3 mL) and heated to 100 °C overnight until the solution became homogeneous. The solvent was removed under reduce pressure to give the desired compound.

4.1.8. Synthetic procedure 7: Ullmann reaction using deanol

A 50 mL round bottom flask was filled with iodobenzene (2.0 mmol), 6-aminocaproic acid (3.0 mmol), CuI (0.20 mmol), $K_3PO_4 \bullet H_2O$ (4.0 mmol), deanol (3.0 mL) and H_2O (5.0 mL). The atmosphere was replaced for nitrogen gas before heating to 80 °C for 48 h. After cooling to room temperature, ice (20 g) was added and the pH was adjusted to 4–5 using an aqueous 1 N HCl solution. This solution was extracted with EtOAc (30 mL, 3 times). The organic layer was washed with brine, and the solvent was removed under reduced pressure. The residue was purified by flash chromatography, eluted with petroleum ether: EtOAc 1:1 (v/v), to obtain the desired compound.

4.1.9. Synthetic procedure 8: Boc deprotection

The Boc-protected amine (0.92 mmol) was dissolved in dry CH_2Cl_2 (6 mL). Subsequently, trifluoroacetic acid (TFA) (1.5 mL) was added. The mixture was stirred for 2 h at room temperature until the solution became homogeneous. The mixture was extracted with and aqueous 1 N NaOH solution (20 mL). The organic layer was collected and dried over $MgSO_4$. The solvent was removed under reduced pressure to obtain the final product.

4.1.10. 4-((phenylamino)methyl)benzoic acid (3a)

The product was obtained using synthetic procedure 1. White solid, yield 53%. ^{1}H NMR (500 MHz, DMSO-d_6) δ 7.89 (d, J = 8.2 Hz, 2H), 7.46 (d, J = 8.2 Hz, 2H), 7.04-7.01 (m, 2H), 6.59–6.49 (m, 3H), 6.33 (br, s, 1H), 4.34 (s, 2H). ^{13}C NMR (126 MHz, DMSO-d_6) δ 167.78, 148.91, 146.11, 130.04, 129.90, 129.76, 129.32, 127.57, 127.52, 116.45, 116.28, 112.81, 112.66, 46.67.

4.1.11. 4-(1-(phenylamino)ethyl)benzoic acid (3b)

The product was obtained using synthetic procedure 1. White solid, yield 45%. ^{1}H NMR (500 MHz, DMSO-d_6) δ 7.86 (d, J = 8.2 Hz, 2H), 7.48 (d, J = 8.3 Hz, 2H), 6.98–6.94 (m, 2H), 6.45-6.43 (m, 3H), 6.21 (d, J = 6.5 Hz, 1H), 4.52 (m, 1H), 1.41 (d, J = 6.8 Hz, 3H). ^{13}C NMR (126 MHz, DMSO-d_6) δ 167.26, 151.40, 147.73, 129.54, 129.42, 128.70(2), 128.67(2), 126.05(2), 112.73(2), 51.95, 24.35.

4.1.12. Methyl 4-(phenylcarbamoyl)benzoate (2c)

The product was obtained using synthetic procedure 2. White solid, yield 80%. ^{1}H NMR (500 MHz, Chloroform-d) δ 8.17–8.12 (m, 2H), 7.93 (d, J = 8.3 Hz, 3H), 7.65 (d, J = 7.9 Hz, 2H), 7.39 (t, J = 8.0 Hz, 2H), 7.18 (t, J = 7.4 Hz, 1H), 3.96 (s, 3H). ^{13}C NMR (126 MHz, DMSO-d_6) δ 166.15, 165.15, 139.53, 139.36, 132.46, 129.63(2), 129.12(2), 128.55(2), 124.41, 120.95(2), 55.03.

4.1.13. 4-(phenylcarbamoyl)benzoic acid (3c)

The product was obtained using synthetic procedure 1. White solid, yield 54%. ^{1}H NMR (500 MHz, DMSO-d_6) δ 10.35 (s, 1H), 8.01 (d, J = 8.0 Hz, 2H), 7.91 (d, J = 8.0 Hz, 2H), 7.82 (d, J = 7.9 Hz, 2H), 7.35 (t, J = 7.7 Hz, 2H), 7.10 (t, J = 7.3 Hz, 1H). ^{13}C NMR (126 MHz, DMSO-d_6) δ 168.23, 165.54, 143.20, 139.21, 134.87, 128.77(2), 128.43(2), 126.63(2), 123.39, 120.23(2).

4.1.14. 4-((methyl(phenyl)amino)methyl)benzoic acid (3d)

The product was obtained using synthetic procedure 1. Yellow solid, yield 75%. ^{1}H NMR (500 MHz, DMSO-d_6) δ 12.89 (s, 1H), 7.89 (d, J = 8.1 Hz, 2H), 7.32 (d, J = 8.1 Hz, 2H), 7.15 (t, J = 7.9 Hz, 2H), 6.70 (d, J = 8.3 Hz, 2H), 6.62 (t, J = 7.1 Hz, 1H), 4.64 (s, 2H), 3.03 (s, 3H). ^{13}C NMR (126 MHz, DMSO-d_6) δ 167.63, 149.35, 145.12, 130.04(2), 129.93, 129.75(2), 129.48(2), 116.53, 112.41(2), 55.70, 39.16.

4.1.15. N-(2-aminophenyl)-4-((phenylamino)methyl)benzamide (4a)

The product was obtained using synthetic procedure 2. Pink solid, yield 36%. ^{1}H NMR (500 MHz, DMSO-d_6) δ 10.58 (s, 1H), 8.10 (d, J = 8.2 Hz, 2H), 7.61 (d, J = 8.1 Hz, 1H), 7.58 (d, J = 8.1 Hz, 2H), 7.53 (d, J = 7.7 Hz, 1H), 7.43 (t, J = 7.6 Hz, 1H), 7.35 (t, J = 7.4 Hz, 1H), 7.20 (t, J = 6.8 Hz, 2H), 7.02–6.74 (m, 3H), 4.47 (s, 2H). ^{13}C NMR (126 MHz, DMSO-d_6) δ 165.66, 148.87, 144.65, 139.02, 133.42, 129.30(2), 128.29(2), 127.30(2), 127.12, 126.90, 124.13, 117.13, 116.85,

116.33, 112.83(2), 46.57. HRMS: $C_{20}H_{20}ON_3$ mass expected $[M+H]^+$ 318.16009, found 318.15988.

4.1.16. N-(2-aminophenyl)-4-(1-(phenylamino)ethyl)benzamide (4b)

The product was obtained using synthetic procedure 2. Yellow solid, yield 30%.^{1}H NMR (500 MHz, Chloroform-*d*) δ 7.89 (s, 1H), 7.83 (d, J = 8.1 Hz, 2H), 7.46 (d, J = 8.2 Hz, 2H), 7.28 (s, 1H), 7.12–7.05 (m, 3H), 6.82 (t, J = 7.2 Hz, 2H), 6.67 (t, J = 7.3 Hz, 1H), 6.48 (d, J = 7.7 Hz, 2H), 4.54 (q, J = 6.8 Hz, 1H), 3.91 (br. s, 2H), 1.53 (d, J = 6.8 Hz, 3H). ^{13}C NMR (126 MHz, Chloroform-*d*) δ 171.19, 149.77, 146.89, 140.73, 132.86(2), 129.17(2), 127.82, 127.19, 126.24(2), 125.23(2), 124.56, 119.73, 118.34, 117.61, 113.33, 53.34, 25.05. HRMS: $C_{21}H_{22}ON_3$, mass expected $[M+H]^+$ 332.17574, found 332.17548.

4.1.17. N_1-(2-aminophenyl)-N_4-phenylterephthalamide (4c)

The product was obtained using synthetic procedure 2. Yellow solid, yield 61%.^{1}H NMR (500 MHz, DMSO-d_6) δ 10.40 (s, 1H), 10.27 (s, 1H), 8.13–8.08 (m, 5H), 7.79 (d, J = 7.7 Hz, 2H), 7.74–7.68 (m, 1H), 7.39–7.34 (dt, J = 10.0, 6.2 Hz, 4H), 7.13 (t, J = 7.2 Hz, 1H). ^{13}C NMR (126 MHz, DMSO-d_6) δ 165.21, 160.46, 139.42, 138.11, 137.27, 131.81, 129.13(2), 128.32(2), 128.19, 128.14(2), 127.28, 126.67, 126.23, 126.53, 124.35, 120.96, 120.84. HRMS: $C_{20}H_{18}O_2N_3$, mass expected $[M+H]^+$ 332.13935, found 332.13913.

4.1.18. N-(2-aminophenyl)-4-((methyl(phenyl)amino)methyl) benzamide (4d)

The product was obtained using synthetic procedure 2. Yellow solid, yield 41%.^{1}H NMR (500 MHz, DMSO-d_6) δ 9.59 (s, 1H), 7.92 (d, J = 8.1 Hz, 2H), 7.32 (d, J = 8.1 Hz, 2H), 7.17–7.13 (m, 3H), 6.98–6.94 (m, 1H), 6.79–6.75 (m, 1H), 6.72 (d, J = 8.1 Hz, 2H), 6.64–6.57 (m, 2H), 4.88 (br. s, 2H), 4.64 (s, 2H), 3.05 (s, 3H). ^{13}C NMR (126 MHz, DMSO-d_6) δ 165.58, 149.37, 143.58, 143.35, 133.61, 129.46(2), 128.48, 128.40, 127.10, 127.04(2), 126.92, 123.77, 116.50, 116.43, 112.61, 112.54, 99.98, 55.66, 39.23. HRMS: $C_{21}H_{22}ON_3$, mass expected $[M+H]^+$ 332.17574, found 332.17563.

4.1.19. (R)- or (S)–N-(1-(4-bromophenyl)ethyl)aniline (7a,b)

The product was obtained using synthetic procedure 4. Yellow solid, yield 32%–33%.^{1}H NMR (500 MHz, Chloroform-*d*) δ 7.50–7.34 (m, 2H), 7.26–7.23 (m, 2H), 7.11–7.07 (m, 2H), 6.67 (t, J = 7.3 Hz, 1H), 6.48 (d, J = 7.9 Hz, 2H), 4.43 (q, J = 6.7 Hz, 1H), 1.50 (d, J = 6.7 Hz, 3H). ^{13}C NMR (126 MHz, Chloroform-*d*) δ 146.74, 144.20, 131.80, 131.73, 129.20, 129.13, 127.69(2), 120.55, 117.68, 113.43(2), 53.25, 24.90.

4.1.20. (R)- or (S)-4-(1-(phenylamino)ethyl)benzonitrile (8a,b)

The product was obtained from (R)- or (S)–*N*-(1-(4-bromophenyl)ethyl)aniline using synthetic procedure 5. Yellow solid, yield 47%–57%. ^{1}H NMR (500 MHz, Chloroform-*d*) δ 7.64–7.59 (m, 2H), 7.51–7.47 (m, 2H), 7.13–7.07 (m, 2H), 6.70–6.67 (m, 1H), 6.46–6.42 (m, 2H), 4.51 (q, J = 6.8 Hz, 1H), 4.08 (br. s, 1H), 1.52 (d, J = 6.8 Hz, 3H). ^{13}C NMR (126 MHz, Chloroform-*d*) δ 151.01, 146.55, 132.70(2), 129.26(2), 126.72(2), 118.93, 117.86, 113.35(2), 110.79, 53.46, 24.97.

4.1.21. (R)- or (S)-4-(1-(phenylamino)ethyl)benzoic acid (9a,b)

The product was obtained from (R)- or (S)-4-(1-(phenylamino) ethyl)benzonitrile using synthetic procedure 6. Yellow solid, yield 57%–97%. ^{1}H NMR (500 MHz, Methanol-d_4) δ 8.03 (d, J = 8.1 Hz, 2H), 7.48 (m, 5H), 7.29 (d, J = 7.5 Hz, 2H), 4.90 (d, J = 6.2 Hz, 1H), 1.79 (d, J = 6.8 Hz, 3H). ^{13}C NMR (126 MHz, Methanol-d_4) δ 165.85, 138.96, 132.68, 130.22(2), 128.49, 128.41, 128.30, 127.67, 126.34(2), 121.42(2), 60.78, 16.01.

4.1.22. (R)- or (S)–N-(2-aminophenyl)-4-(1-(phenylamino)ethyl) benzamide (10a,b)

The product was obtained from (R)- or (S)-4-(1-(phenylamino) ethyl)benzoic acid using synthetic procedure 2. Yellow solid, yield 30%–32%. The (S)–*N*-(2-aminophenyl)-4-(1-(phenylamino)ethyl) benzamide $[\alpha]^{20}_D$ (c = 1, CH_2Cl_2) = −8.6; (R)-*N*-(2-aminophenyl)-4-(1-(phenylamino)ethyl)benzamide $[\alpha]^{20}_D$(c = 1, CH_2Cl_2) = +8.5.

4.1.23. 6-(phenylamino)hexanoic acid (12a)

The product was obtained using synthetic procedure 7. Yellow solid, yield 16%. ^{1}H NMR (500 MHz, Chloroform-*d*) δ 7.19–7.16 (m, 2H), 6.71 (t, J = 7.3 Hz, 1H), 6.62 (d, J = 7.8 Hz, 2H), 3.12 (d, J = 7.2 Hz, 2H), 2.38 (t, J = 7.4 Hz, 2H), 1.72–1.62 (m, 5H), 1.50–1.43 (m, 2H). ^{13}C NMR (126 MHz, Chloroform-*d*) δ 179.16, 148.14, 129.26(2), 117.50, 112.97(2), 43.88, 33.87, 29.14, 26.59, 24.45.

4.1.24. Tert-butyl (2-(5-(phenylamino)pentanamido)phenyl) carbamate (14a)

The product was obtained using synthetic procedure 2. Yellow solid, yield 46%. ^{1}H NMR (500 MHz, Chloroform-*d*) δ 8.02 (br. s, 1H), 7.55–7.51 (m, 1H), 7.39 (d, J = 8.7 Hz, 1H), 7.33 (q, J = 5.0 Hz, 1H), 7.19–7.14 (m, 3H), 6.74 (br. s, 1H), 6.69 (t, J = 7.3 Hz, 1H), 6.59 (d, J = 7.9 Hz, 1H), 6.37 (d, J = 8.7 Hz, 1H), 3.15–3.08 (m, 2H), 2.42–2.39 (m, 2H), 1.82–1.71 (m, 2H), 1.69–1.63 (m, 2H), 1.52–1.48 (m, 11H).^{13}C NMR (126 MHz, Chloroform-*d*) δ 204.06, 171.86, 148.37, 130.36, 129.25(2), 126.18, 125.74, 124.52, 121.59, 117.20(2), 112.72(2), 81.11, 43.72, 37.27, 29.24, 28.30(3), 26.71, 25.45.

4.1.25. Tert-butyl (2-(6-oxo-6-phenylhexanamido)phenyl) carbamate(14b)

The product was obtained using synthetic procedure 2. Yellow solid, yield 66%. ^{1}H NMR (500 MHz, Chloroform-*d*) δ 8.30 (br. s, 1H), 7.97–7.92 (m, 2H), 7.59–7.55 (m, 1H), 7.47–7.40 (m, 4H), 7.16–7.10 (m, 1H), 7.08 (br. s, 1H), 2.99 (t, J = 7.3 Hz, 2H), 2.38 (t, J = 7.5 Hz, 2H), 1.80–1.74 (m, 4H), 1.49 (s, 9H), 1.47–1.41 (m, 2H). ^{13}C NMR (126 MHz, Chloroform-*d*) δ 200.39, 172.25, 154.22, 136.92, 133.05, 130.79, 130.06, 128.61(2), 128.04(2), 126.14, 125.35, 124.53(2), 80.83, 38.28, 36.95, 28.75, 28.32(3), 25.50, 23.75.

4.1.26. Tert-butyl (2-(5-oxo-5-(phenylamino)pentanamido)phenyl) carbamate(14c)

The product was obtained using synthetic procedure 2. Yellow solid, yield 66%. ^{1}H NMR (500 MHz, Chloroform-*d*) δ 8.49 (br. s, 1H), 7.80–7.77 (m, 2H), 7.50–7.37 (m, 5H), 7.18–7.07 (m, 3H), 6.67 (br. s, 1H), 3.46 (q, J = 6.5 Hz, 2H), 2.44 (t, J = 7.1 Hz, 2H), 1.82–1.76 (m, 2H), 1.71–1.65 (m, 2H), 1.48 (s, 9H). ^{13}C NMR (126 MHz, Chloroform-*d*) δ 172.70, 168.22, 154.57, 134.80, 131.87, 131.17, 130.29, 128.95, 127.33(2), 126.57, 125.67, 125.54(2), 124.91, 81.25, 39.59, 36.58, 29.19, 28.68(3), 23.01.

4.1.27. N-(2-aminophenyl)-5-(phenylamino)pentanamide(15a)

The product was obtained using synthetic procedure 8. Yellow solid, yield 90%.^{1}H NMR (500 MHz, DMSO-d_6) δ 9.10 (s, 1H), 7.15 (d, J = 8.8 Hz, 1H), 7.04 (t, J = 7.8 Hz, 2H), 6.88 (t, J = 8.2 Hz, 1H), 6.71 (d, J = 9.0 Hz, 1H), 6.54–6.47 (m, 4H), 5.51 (t, J = 5.6 Hz, 1H), 4.81 (s, 2H), 2.98 (q, J = 6.8 Hz, 2H), 2.32 (t, J = 7.4 Hz, 2H), 1.66–1.54 (m, 4H), 1.44–1.38 (m, 2H). ^{13}C NMR (126 MHz, Chloroform-*d*) δ 171.55, 148.36, 140.75, 129.27(2), 127.24, 125.17, 124.36, 119.66, 118.35, 117.23, 112.74(2), 43.68, 36.88, 29.22, 26.74, 25.51.

4.1.28. N-(2-aminophenyl)-6-oxo-6-phenylhexanamide(15b)

The product was obtained using synthetic procedure 8. Yellow solid, yield 96%. ^{1}H NMR (500 MHz, DMSO-d_6) δ 9.09 (s, 1H), 7.97 (d, J = 7.1 Hz, 2H), 7.63 (t, J = 7.4 Hz, 1H), 7.52 (t, J = 7.7 Hz, 2H), 7.14 (d, J = 9.1 Hz, 1H), 6.88 (t, J = 8.3 Hz, 1H), 6.70 (d, J = 9.2 Hz, 1H), 6.52 (t,

$J = 8.2$ Hz, 1H), 4.81 (br. s, 2H), 3.04 (t, $J = 7.2$ Hz, 2H), 2.32 (t, $J = 7.4$ Hz, 2H), 1.73–1.57 (m, 4H), 1.31–1.35 (m, 2H). ^{13}C NMR (126 MHz, DMSO-d_6) δ 200.56, 171.56, 142.36, 137.19, 133.50, 129.87, 129.22(2), 128.33(2), 126.14, 125.78, 124.00, 116.27, 38.28, 36.12, 28.77, 25.67, 24.05.

4.1.29. N-(5-((2-aminophenyl)amino)-5-oxopentyl) benzamide(15c)

The product was obtained using synthetic procedure 8. Yellow solid, yield 72%. ^{1}H NMR (500 MHz, DMSO-d_6) δ 9.10 (s, 1H), 8.49 (t, $J = 5.3$ Hz, 1H), 7.84 (d, $J = 7.3$ Hz, 2H), 7.51 (t, $J = 7.3$ Hz, 1H), 7.45 (t, $J = 7.4$ Hz, 2H), 7.15 (d, $J = 7.7$ Hz, 1H), 6.88 (t, $J = 7.6$ Hz, 1H), 6.70 (d, $J = 7.9$ Hz, 1H), 6.52 (t, $J = 7.5$ Hz, 1H), 4.83 (s, 2H), 3.29 (q, $J = 6.3$ Hz, 2H), 2.35 (t, $J = 7.2$ Hz, 2H), 1.67–1.54 (m, 4H). ^{13}C NMR (126 MHz, DMSO-d_6) δ 171.52, 166.56, 142.35, 135.15, 131.51, 128.70(2), 127.68, 127.54, 125.76, 126.18(2), 123.98, 116.30, 39.52, 35.94, 29.31, 23.37.

4.2. HDAC inhibition study

Black 96-well flat bottom microplates (Corning® Costar®, Corning Incorporated, NY) were used. Human recombinant C-terminal FLAG-tag, C-terminal His-tag HDAC 1 (BPS Bioscience, Catalog #: 50051), human recombinant C-terminal FLAG-tag HDAC 2 (BPS Bioscience, Catalog #: 50052) or human recombinant C-terminal His-tag HDAC 3/NcoR2 (BPS Bioscience, Catalog #: 50003) were diluted in incubation buffer (25 mM Tris-HCl, pH 8.0, 137 mM NaCl, 2.7 mM KCl, 1 mM MgCl, 0.01% Triton-X and 1 mg/mL BSA). 40 μL of this dilution was incubated with 10 μL of different concentrations of inhibitors in 10% DMSO/incubation buffer and 50 μL of the fluorogenic Boc-Lys(ε-Ac)-AMC (20 mM, Bachem, Germany) at 37 °C. After 90 min incubation time 50 μL of the stop solution (25 mM Tris-HCl (pH 8), 137 mM NaCl, 2.7 mM KCl, 1 mM $MgCl_2$, 0.01% Triton-X, 6.0 mg/mL trypsin (porcine pancreas Type IX-S, lyophilized powder, 13,000–20,000 BAEE units/mg protein, Sigma Aldrich) and 200 μM vorinostat) was added. After a following incubation at 37 °C for 30 min, the fluorescence was measured on a Synergy H1 Platereader (BioTek, USA) with a gain of 70 and an excitation wavelength of 370 nm and an emission wavelength of 460 nm. GraphPad Prism 5.0 (GraphPad Software, Inc.) was used for the determination of the IC_{50} of each inhibitor. Nonlinear regression was used for data fitting.

4.3. Docking study

Docking studies where performed to get insight in the structure activity relationships. All molecular handlings were done with the program Discovery studio (Dassault systèmes) version 2018 and the crystal structures of human HDAC 1 (PDB-code:5ICN), human HDAC 2 (PDB-code: 4LY1) and human HDAC 3 (PDB-code: 4A69).

The CDOCKER protocol was used for docking which is a CHARMm based algorithm. Docking was verified by use of the ligand (4-(acetylamino)-*N*-[2-amino-5-(thiophen-2-yl)phenyl] benzamide) from de crystal structure 4LY1. This ligand contains the zinc-binding group and the linker group also present in our molecules. First, the ligand was removed from 4LY1 and subsequently docked back in the crystal structure. All 10 poses given show a comparable position compared to the original pose from the crystal structure.

Also the ligand was placed in HDAC 1 and HDAC 3 after superimposing HDAC 1 and HDAC 3 with HDAC 2 at the Cα carbon atoms of the backbone. The position of the o-aminoanilide core was used as a reference to evaluate the dockings in the HDAC active sites. Docked poses from all the compounds where the NH_2 from the zinc-binding group did not face the zinc in the same fashion as the reference, were discarded. Poses with the lowest CDOCKER energies were chosen.

4.4. Cell viability

4.4.1. Cell culture

RAW264.7 macrophages were obtained from the American Type Culture Collection (ATCC; Wesel, Germany) and cultured in 96-well plate or flasks (Costar Europe, Badhoevedorp, The Netherlands) at 37 °C under 5% CO_2/95% air in Dulbecco's Modification of Eagle's Medium (DMEM) containing GlutaMAX™ (Gibco® by life Technologies, Bleiswijk, The Netherlands) supplemented with 10% (v/v) heated fetal bovine serum (FBS; Invitrogen, Breda, The Netherlands), 2 mM additional GlutaMAX™ (Gibco® by life Technology, Bleiswijk, The Netherlands), 100 U/ml penicillin (Gibco® by life Technologies, Bleiswijk, The Netherlands) and 100 μg/ml streptomycin (Gibco® by life Technologies, Bleiswijk, The Netherlands). RAW 264.7 cells were used between passage 5 and 16.

4.4.2. MTS assay

RAW264.7 cells were seeded in 96-well plate at the concentration of 25,000 cells/cm^2. The next day, medium was replaced with fresh medium containing HDAC inhibitors at the indicated concentrations. After 24 h incubation at 37 °C, 20 μl CellTiter 96 AQ_{ueous} One Solution reagent (Promega) was added to each well. The cells were incubated at 37 °C for 2 h in dark. The absorbance at 490 nM was measured using an Synergy H1 plate reader. The results were plotted as % of control.

4.5. NF-κB activation

RAW-Blue™ cells (InvivoGen, San Diego, CA, USA) are derived from RAW264.7 macrophages. The secreted embryonic alkanline phosphatase (SEAP) is detected using SEAP detection medium (QUANTI-Blue™). RAW-Blue cells were seeded at a concentration around 550,000 cells/mL. The cells were treated with 10 ng/mL LPS/IFNγ for 4 h, after the pre-incubation with HDAC inhibitors for 16 h. The detection medium (QUANTI-BLUE) was prepared according to the manufacturer's protocol. 20 μl cell supernatant was added into 180 μL detection medium and incubated at 37 °C for 3 h. The SEAP activity was measured using a Synergy H1 plate reader with absorbance at 650 nm. The results were plotted as % of control. RAW-Blue cells were used between passage 4 to 14.

4.6. RT-qPCR

RAW264.7 cells were washed twice with Dulbecco's Phosphate-buffered Saline (DPBS, Gibco® by life Technologies, Bleiswijk, The Netherlands) and total RNA was isolated by Maxwell® 16 LEV simplyRNA Tissue Kit (Promega) according to the manufacturer's protocol. RNA concentration(OD260) and purity (OD260/OD280) were measured by NanoDrop ND-1000 UV–Vis spectrophotometer (NanoDrop Technologies, Wilmington, DE, USA). Then, RNA was reverse transcribed to cDNA using the Reverse Transcription Kit (#A3500, Promega). 10 ng of cDNA, 5 μL 2× SensiMix SYBR Lo-ROX and 0.4 μL primers were applied for each RT-qPCR, which was performed on a QuantStudio(TM) 7 Flex System. For each sample, the real-time PCR were performed in duplicate. Data analysis was performed with QuantStudio™ Real-Time PCR Software. Gene expression levels were normalized to the expression of the reference gene glyceralde-3-phosphate dehydrogenase (GAPDH), which was not influenced by the experimental conditions resulting in the ΔC_t value. Gene expression levels were calculated by the comparative C_t method ($2^{-\Delta\Delta Ct}$) [28].

Primers for qRT-PCR were as follows

GAPDH forward, 5′- ACAGTCCATGCCATCACTGC-3’;
GAPDH reverse, 5′- GATCCACGACGGACACATTG-3’;
IL-10 forward, 5′- ATAACTGCACCCACTTCCCAGTC-3’;
IL-10 reverse, 5′- CCCAAGTAACCCTTAAAGTCCTGC-3’;
IL-6 forward, 5′- TGATGCTGGTGACAACCACGGC-3’;
IL-6 reverse, 5′- TAAGCCTCCGACTTGTGAAGTGGTA-3’;
TNFα forward, 5′- CATCTTCTCAAAATTCGAGTGACAA-3’;
TNFα reverse, 5′- GAGTAGACAAGGTACAACCC-3’;
miNOS forward, 5′- CTATCAGGAAGAAATGCAGGAGAT-3’;
miNOS reverse, 5′- GAGCACGCTGAGTACCTCATT-3’;

Conflicts of interest

The authors declare no conflict of interest.

Acknowledgement

We acknowledge the China Scholarship Council (CSC) for providing a scholarship to Fangyuan Cao (file number 201606170109).

Appendix A. Supplementary data

Supplementary data to this article can be found online at https://doi.org/10.1016/j.ejmech.2019.05.038.

References

[1] N.G.J. Leus, M.R.H. Zwinderman, F.J. Dekker, Histone deacetylase 3 (HDAC 3) as emerging drug target in NF-κB-mediated inflammation, Curr. Opin. Chem. Biol. 33 (2016) 160–168, https://doi.org/10.1016/j.cbpa.2016.06.019.
[2] M. Haberland, R.L. Montgomery, E.N. Olson, The many roles of histone deacetylases in development and physiology: implications for disease and therapy, Nat. Rev. Genet. 10 (2009) 32–42, https://doi.org/10.1038/nrg2485.
[3] H.-T. Qin, H.-Q. Li, F. Liu, Selective histone deacetylase small molecule inhibitors: recent progress and perspectives, Expert Opin. Ther. Pat. 27 (2016) 1–15, https://doi.org/10.1080/13543776.2017.1276565.
[4] E. Seto, M. Yoshida, Erasers of histone acetylation: the histone deacetylase enzymes, Cold Spring Harb. Perspect. Biol. 6 (2014), https://doi.org/10.1101/cshperspect.a018713.
[5] M. Dokmanovic, C. Clarke, P.A. Marks, Histone deacetylase inhibitors: overview and perspectives, Mol. Cancer Res. 5 (2007) 981–989, https://doi.org/10.1158/1541-7786.MCR-07-0324.
[6] E.E. Hull, M.R. Montgomery, K.J. Leyva, HDAC Inhibitors as Epigenetic Regulators of the Immune System : Impacts on Cancer Therapy and Inflammatory Diseases, 2016, p. 2016, https://doi.org/10.1155/2016/8797206.
[7] A.G. Kazantsev, L.M. Thompson, Therapeutic application of histone deacetylase inhibitors for central nervous system disorders, Nat. Rev. Drug Discov. 7 (2008) 854–868, https://doi.org/10.1038/nrd2681.
[8] N.G.J. Leus, T. van den Bosch, P.E. van der Wouden, K. Krist, M.E. Ourailidou, N. Eleftheriadis, L.E.M. Kistemaker, S. Bos, R.A.F. Gjaltema, S.A. Mekonnen, R. Bischoff, R. Gosens, H.J. Haisma, F.J. Dekker, HDAC1-3 inhibitor MS-275 enhances IL10 expression in RAW264.7 macrophages and reduces cigarette smoke-induced airway inflammation in mice, Sci. Rep. 7 (2017) 45047, https://doi.org/10.1038/srep45047.
[9] A. Villagra, E.M. Sotomayor, E. Seto, Histone deacetylases and the immunological network: implications in cancer and inflammation, Oncogene 29 (2010) 157–173, https://doi.org/10.1038/onc.2009.334.
[10] R. Glauben, E. Sonnenberg, M. Zeitz, B. Siegmund, HDAC inhibitors in models of inflammation-related tumorigenesis, Cancer Lett. 280 (2009) 154–159, https://doi.org/10.1016/j.canlet.2008.11.019.
[11] M.R. Shakespear, M.A. Halili, K.M. Irvine, D.P. Fairlie, M.J. Sweet, Histone deacetylases as regulators of inflammation and immunity, Trends Immunol. 32 (2011) 335–343, https://doi.org/10.1016/j.it.2011.04.001.
[12] M. Conte, R. De Palma, L. Altucci, HDAC inhibitors as epigenetic regulators for cancer immunotherapy, Int. J. Biochem. Cell Biol. 98 (2018) 65–74, https://doi.org/10.1016/j.biocel.2018.03.004.
[13] S. Aspeslagh, D. Morel, J.C. Soria, S. Postel-Vinay, Epigenetic modifiers as new immunomodulatory therapies in solid tumours, Ann. Oncol. 29 (2018) 812–824, https://doi.org/10.1093/annonc/mdy050.
[14] M.D. Cantley, D.R. Haynes, Epigenetic regulation of inflammation: progressing from broad acting histone deacetylase (HDAC) inhibitors to targeting specific HDACs, Inflammopharmacology 21 (2013) 301–307, https://doi.org/10.1007/s10787-012-0166-0.
[15] A. Shapouri-Moghaddam, S. Mohammadian, H. Vazini, M. Taghadosi, S.A. Esmaeili, F. Mardani, B. Seifi, A. Mohammadi, J.T. Afshari, A. Sahebkar, Macrophage plasticity, polarization, and function in health and disease, J. Cell. Physiol. 233 (2018) 6425–6440, https://doi.org/10.1002/jcp.26429.
[16] F.J. Dekker, T. Van Den Bosch, N.I. Martin, Small molecule inhibitors of histone acetyltransferases and deacetylases are potential drugs for inflammatory diseases, Drug Discov. Today 19 (2014) 654–660, https://doi.org/10.1016/j.drudis.2013.11.012.
[17] Z. Lu, R.J. Twieg, Copper-catalyzed aryl amination in aqueous media with 2-dimethylaminoethanol ligand, Tetrahedron Lett. 46 (2005) 2997–3001, https://doi.org/10.1016/j.tetlet.2005.03.027.
[18] M.E. Ourailidou, N.G.J. Leus, K. Krist, A. Lenoci, A. Mai, F.J. Dekker, Chemical epigenetics to assess the role of HDAC1-3 inhibition in macrophage pro-inflammatory gene expression, Medchemcomm 7 (2016) 2184–2190, https://doi.org/10.1039/c6md00375c.
[19] N. Khan, M. Jeffers, S. Kumar, C. Hackett, F. Boldog, N. Khramtsov, X. Qian, E. Mills, S.C. Berghs, N. Carey, P.W. Finn, L.S. Collins, A. Tumber, J.W. Ritchie, P.B. Jensen, H.S. Lichenstein, M. Sehested, Determination of the class and isoform selectivity of small-molecule histone deacetylase inhibitors, Biochem. J. 409 (2008) 581–589, https://doi.org/10.1042/BJ20070779.
[20] C.J. Chou, D. Herman, J.M. Gottesfeld, Pimelic diphenylamide 106 is a slow, tight-binding inhibitor of class I histone deacetylases, J. Biol. Chem. 283 (2008) 35402–35409, https://doi.org/10.1074/jbc.M807045200.
[21] B.E.L. Lauffer, R. Mintzer, R. Fong, S. Mukund, C. Tam, I. Zilberleyb, B. Flicke, A. Ritscher, G. Fedorowicz, R. Vallero, D.F. Ortwine, J. Gunzner, Z. Modrusan, L. Neumann, C.M. Koth, J.S. Kaminker, C.E. Heise, P. Steiner, Histone deacetylase (HDAC) inhibitor kinetic rate constants correlate with cellular histone acetylation but not transcription and cell viability, J. Biol. Chem. 288 (2013) 26926–26943, https://doi.org/10.1074/jbc.M113.490706.
[22] F.F. Wagner, M. Lundh, T. Kaya, P. McCarren, Y.L. Zhang, S. Chattopadhyay, J.P. Gale, T. Galbo, S.L. Fisher, B.C. Meier, A. Vetere, S. Richardson, N.G. Morgan, D.P. Christensen, T.J. Gilbert, J.M. Hooker, M. Leroy, D. Walpita, T. Mandrup-Poulsen, B.K. Wagner, E.B. Holson, An isochemogenic set of inhibitors to define the therapeutic potential of histone deacetylases in β-cell protection, ACS Chem. Biol. 11 (2016) 363–374, https://doi.org/10.1021/acschembio.5b00640.
[23] J.C. Bressi, A.J. Jennings, R. Skene, Y. Wu, R. Melkus, R. De Jong, S. O'Connell, C.E. Grimshaw, M. Navre, A.R. Gangloff, Exploration of the HDAC2 foot pocket: synthesis and SAR of substituted N-(2-aminophenyl)benzamides, Bioorg. Med. Chem. Lett 20 (2010) 3142–3145, https://doi.org/10.1016/j.bmcl.2010.03.091.
[24] J.L. Methot, P.K. Chakravarty, M. Chenard, J. Close, J.C. Cruz, W.K. Dahlberg, J. Fleming, C.L. Hamblett, J.E. Hamill, P. Harrington, A. Harsch, R. Heidebrecht, B. Hughes, J. Jung, C.M. Kenific, A.M. Kral, P.T. Meinke, R.E. Middleton, N. Ozerova, D.L. Sloman, M.G. Stanton, A.A. Szewczak, S. Tyagarajan, D.J. Witter, J. Paul Secrist, T.A. Miller, Exploration of the internal cavity of histone deacetylase (HDAC) with selective HDAC1/HDAC2 inhibitors (SHI-1:2), Bioorg. Med. Chem. Lett 18 (2008) 973–978, https://doi.org/10.1016/j.bmcl.2007.12.031.
[25] D.J. Witter, P. Harrington, K.J. Wilson, M. Chenard, J.C. Fleming, B. Haines, A.M. Kral, J.P. Secrist, T.A. Miller, Optimization of biaryl selective HDAC1&2 inhibitors (SHI-1:2), Bioorg. Med. Chem. Lett 18 (2008) 726–731, https://doi.org/10.1016/j.bmcl.2007.11.047.
[26] X. Chen, I. Barozzi, A. Termanini, E. Prosperini, A. Recchiuti, J. Dalli, F. Mietton, G. Matteoli, S. Hiebert, G. Natoli, Requirement for the histone deacetylase Hdac3 for the inflammatory gene expression program in macrophages, Proc. Natl. Acad. Sci. Unit. States Am. 109 (2012) E2865–E2874, https://doi.org/10.1073/pnas.1121131109.
[27] N.G.J. Leus, P.E. Van Der Wouden, T. Van Den Bosch, W.T.R. Hooghiemstra, M.E. Ourailidou, L.E.M. Kistemaker, R. Bischoff, R. Gosens, H.J. Haisma, F.J. Dekker, HDAC 3-selective inhibitor RGFP966 demonstrates anti-inflammatory properties in RAW 264.7 macrophages and mouse precision-cut lung slices by attenuating NF-κB p65 transcriptional activity, Biochem. Pharmacol. 108 (2016) 58–74, https://doi.org/10.1016/j.bcp.2016.03.010.
[28] K.J. Livak, T.D. Schmittgen, Analysis of relative gene expression data using real-time quantitative PCR and the 2-ΔΔCT method, Methods 25 (2001) 402–408, https://doi.org/10.1006/meth.2001.1262.